Int. J. Electron. Commun. (AEÜ) 126 (2020) 153465

Contents lists available at ScienceDirect

International Journal of Electronics and Communications

journal homepage: www.elsevier.com/locate/aeue

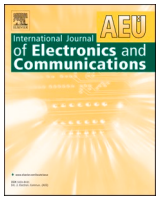

Regular paper

Design and analysis of low profile and low SAR full-textile UWB wearable antenna with metamaterial for WBAN applications

Husnu Yalduz [a], Timucin Emre Tabaru [b,*], Veli Tayfun Kilic [c], Mustafa Turkmen [d]

[a] Dept. of Electronics and Automation, Hitit Unv., Voc. High School, 19169 Corum, Turkey
[b] Clinical Engineering Research and Application Center, Erciyes Unv., 38039 Kayseri, Turkey
[c] Dept. of Electrical and Electronics Engineering, Abdullah Gul Unv., 38039 Kayseri, Turkey
[d] Dept. of Electrical and Electronics Engineering, Erciyes Unv., 38039 Kayseri, Turkey

ARTICLE INFO

Keywords:
Wireless body area network
Ultra-wideband antenna
Metamaterial
Textile antenna

ABSTRACT

In this paper, a low-profile wearable antenna with metamaterial (MM) for wireless body area network (WBAN) applications is presented. The designed antenna with MM operates in the ultra-wideband (UWB) between 4.55 and 13 GHz and it has a thickness of 4.68 mm. To the best of our knowledge, it is the lowest thickness reported in the literature for UWB antennas with MM. The proposed is designed and manufactured using fully flexible textiles. The designed antenna was simulated in free space and on the human body model. Simulation results show that gain, directionality, and front-to-back ratio of the antenna increase considerably with the placement of the MM. Also, in simulations, it is found that the specific absorption rate (SAR) values for the designed antenna reduce by 98.3% when MM is used. These SAR values calculated for the designed antenna with MM are well below the limits defined in European standards. The designed antenna and metamaterials were manufactured, too, and scattering parameters were measured. Measurement results are in good agreement with the results found in the simulations. It shows that the proposed antenna is very suitable for use in WBAN applications due to its low thickness, having low SAR, and UWB operation.

1. Introduction

Recently, wearable textile antennas have attracted great interests of researchers from both academia and industry because of wide range of their usages as a part of wireless body area network (WBAN) systems such as in sport, security, health, and military applications [1]. Wearable textile antennas are preferred to be used in WBAN applications because they offer important advantages that include having low cost and low production complexity, being lightweight, providing high flexibility, and easy integration into the garment [2]. Lately, various flexible and textile wearable antenna configurations such as planar monopole [3,4], planar inverted-F shaped [5,6], fractal [7], reconfigurable [8], and substrate-integrated wave guide (SIW) [9] antennas have been proposed in literature. However, these antennas suffer from either narrow bandwidth or low gain. For WBAN systems usually it is preferred to operate on ultra-wideband (UWB) frequency spectrum that was determined by the Federal Communications Commission (FCC) in 2002 [10].

In wearable antenna designs textiles are good choices to be used as substrate because of their low dielectric permittivity, which increases the antenna impedance bandwidth [11,12], and among various fabrics felt [3,9] and denim [12–15] are widely used types. In addition, using a partial ground plane at the back of the substrate impedance bandwidth is further increased. In our designed antenna, to increase the bandwidth we also used felt as substrate material and placed a partial ground plane at the back of the substrate. On the other hand, another problem observed while usage of wearable antennas is low gain. These antennas are generally designed for use on a body. However, antenna performance values such as directionality, gain and efficiency degrade when the antenna is in close proximity to the body. Moreover, with placement of an antenna on a body, electromagnetic waves radiated from the antenna penetrate more into the body that results in increased system specific absorption rate (SAR) value. To prevent interactions between the antenna and the body one method is to integrate metamaterial (MM) structures at the back of the antenna. MM structures are used as reflectors to improve the performance and reduce the overall thickness of

* Corresponding author.
E-mail addresses: husnuyalduz@hitit.edu.tr (H. Yalduz), etabaru@erciyes.edu.tr (T.E. Tabaru), tayfun.kilic@agu.edu.tr (V.T. Kilic), mturkmen@erciyes.edu.tr (M. Turkmen).

https://doi.org/10.1016/j.aeue.2020.153465
Received 7 May 2020; Accepted 14 September 2020
Available online 18 September 2020

the traditional patch antenna for single-band [14,16], dual band [5,7,12,15,17], and wideband usages [6,18–20]. Besides, in literature there are designs where MM structures are not used as reflectors, but they are used as electromagnetic coupling prohibitive between antennas and inductive surface [21,22].

In this study, to overcome aforementioned problems, a wearable full-textile UWB antenna made of felt substrate and nickel-copper-polyester conductor fabric tape that are placed on a partial ground plane integrated with designed MM structure at the back is introduced for WBAN applications. The designed antenna with the MM structure has 4.68 mm thickness, which is the lowest thickness reported in literature for UWB antennas with a MM until now. Performance of the designed low-profile antenna was first investigated with comparative three-dimensional (3D) electromagnetic (EM) simulations with and without the MM at the back of the antenna in free space and on human body model. Results show that, with placement of the designed MM structure at the back of the antenna performance parameters of gain, directionality, and front-to-back ratio (FBR) improve substantially, whereas interaction between fields radiated from the antenna and the human body is prevented. The designed antenna and the MM structure were successfully manufactured, and measurements were obtained, too. Measurement results are in good agreement with the results found in simulations. The proposed antenna with MM structure promising to be used for WBAN applications is proved to operate in ultra-wide frequency band with a very low SAR value while having very small thickness despite its complete flexibility.

2. Antenna and metamaterial structure design

2.1. Antenna design

We started our designs with the antenna part. The antenna is located on a felt substrate in sizes of 80 mm length, 61 mm width, and 1 mm height with a relative permittivity of 1.4 and a loss tangent of 0.04. The radiator patch and ground plane metallic layers, on the other hand, are made of 0.17 mm thick nickel-copper-polyester tape with an approximate conductivity of $1.18x10^5$ S/m. Structure of the designed wearable microstrip antenna and its geometrical parameters are shown in Fig. 1 (a) from front and back views. In the figure, substrate and metallic layers are represented with red and magenta, respectively. Also, connector in contact with the feed line is shown with yellow color. As seen, the antenna consists of a hexagonal radiating patch and a microstrip feed on the front side of the felt substrate. The hexagonal radiator patch geometry of the proposed antenna has been presented and investigated before in literature [3]. However, at the back side of the substrate there is a rectangular ground plane and a circular parasitic patch, which increases the antenna bandwidth.

In Fig. 1(a), length and width of the substrate are depicted with L_s and W_s, respectively. Similarly, length and width of the antenna are labeled as L_p and W_p, respectively. Also, Wf and L_f stand for width and length of the feed line, respectively, and w and l represent lengths of straight edges of the hexagonal antenna geometry at the top and side. On the other hand, at the back side of the antenna width and length of the rectangular ground plane are pointed out with W_g and L_g, respectively. Also, r and g stand for radius of the circular parasitic patch and distance between the rectangular ground plane and the circular parasitic patch, respectively.

All the geometrical parameters of the antenna that are represented in Fig. 1(a) were optimized by means of an electromagnetic simulation tool by taking into account the antenna bandwidth. After that, the antenna was manufactured with sizes equal to optimum antenna geometries. The optimized antenna parameters are given in Table 1 and the manufactured antenna with optimum sizes is illustrated from front and back views in Fig. 1(b). As seen in the table, width of the feed line (W_f) is 3.85 mm, which enables characteristic impedance of the microstrip feed line to be equal to 50 Ω in the operating frequency band.

2.2. Metamaterial structure design

After optimizing the antenna, we designed MM structure and integrated it to the back of the antenna to reduce the interaction between the antenna and a human body. In the designed system while constructing the MM structure reflection coefficient, i.e., S_{11} parameter, over the whole UWB operation frequency band is the main concern. In the design, felt material having a thickness of 1 mm is placed between the MM and the antenna as a spacer for fixing the distance and preventing electrical contact between the MM and the antenna. Fig. 2(a) shows the cross-section view of the antenna with the MM. As seen in the cross-section view, the MM structure consists of three layers that are two metallic (metasurface and ground plane) layers and a dielectric substrate between them. As in the antenna design, in the MM structure nickel-copper-polyester fabric and felt fabric are used for the metallic layers and the dielectric substrate, respectively. However, different from the antenna felt and felt spacer, felt fabric used in the MM structure has 2 mm thickness. The MM cell sizes have been optimized with simulations. Fig. 2(b) shows the detailed geometry of the proposed metasurface structure that consists of square shape unit cells with a number of 49 in total aligned in a 7x7 square lattice. The reason for choosing a square shape lattice for the metasurface is its ease of production. As seen in the figure, width (W_d) and length (L_d) of the MM structure equal to 100 mm, whereas each metasurface cell has 10 mm side lengths, i.e., both W_m and

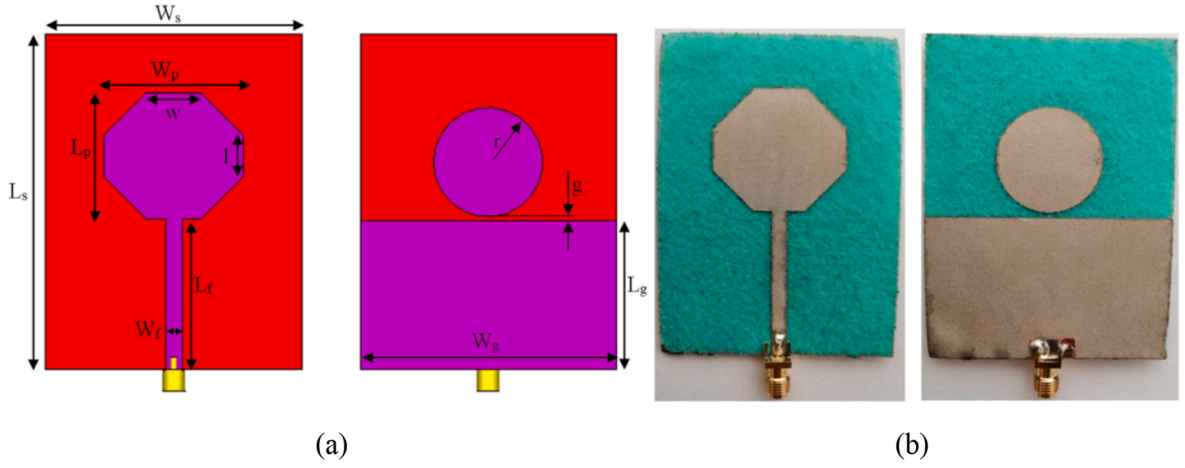

Fig. 1. (a) Proposed antenna architecture from front and back views together with its geometrical parameters, (b) photos of the manufactured antenna with optimum sizes from front and back views.

Table 1
Optimized geometric parameters of the proposed antenna (mm).

W_s	Ls	W_p	L_p	w	l	W_f	L_f	W_g	L_g	r	g	h_{sub}
61	80	33	30	13	10	3.85	33.5	61	33	13	0.5	1

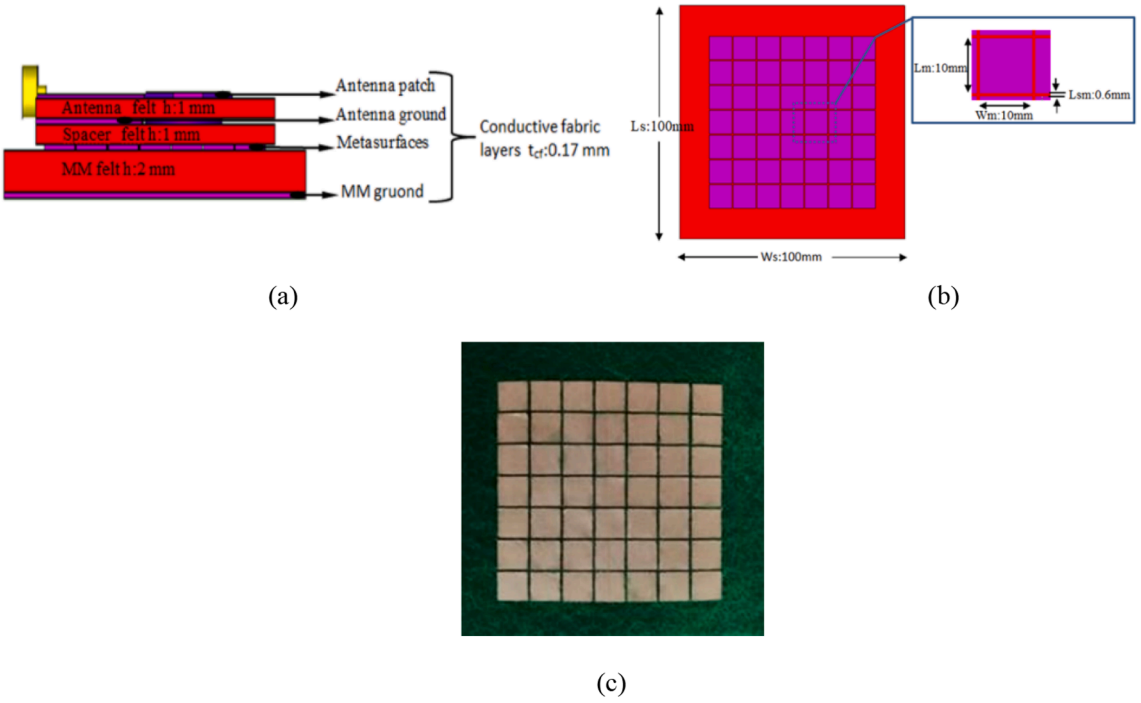

Fig. 2. (a) Side view of the proposed structure, where antenna structure consisting of patch, felt and ground from top to bottom is placed at top and spacer is sandwiched between the antenna and the metamaterial structure that includes metasurfaces, felt and ground layers from top down, (b) proposed metasurface structure consisting of 49 metasurface cells in total that are aligned in 7x7 square lattice together with detailed cell geometry in inset, (c) fabricated prototype of the designed MM structure.

L_m are 10 mm, and these unit cells are 0.6 mm (L_{sm}) apart from each other. Fig. 2(c) shows the manufactured prototype of the MM structure. On the ultra-wide frequency band between 1 GHz and 15 GHz calculated in simulations for the optimized MM structure, the variation of the reflection phase is given in Fig. 3(a). In Fig. 3(b), on the other hand, the simulation model expressing the boundary conditions of the unit cell is shown. Because of periodic placement of the metasurface cells periodic boundary condition is used in the simulations.

In addition, the designed MM structure was simulated, and the permeability, permeability, and hence refractive index values of the structure calculated from the calculated S-parameters were calculated on the working frequency band of the antenna. Variations of real and imaginary parts of permittivity, permeability, and refractive index calculated for the designed MM structure are shown in Figs. 4–6, respectively. As seen in Fig. 4, there is a resonance of permeability in frequency around 11.5 GHz. On the other hand, the real part of the permittivity is negative at frequencies lower than 6.8 GHz approximately. At frequencies between 6.8 GHz and 11.5 GHz real part of the permittivity is positive and after 11.5 GHz it again falls below 0. In short, the designed MM structure has a negative real part of the permittivity at

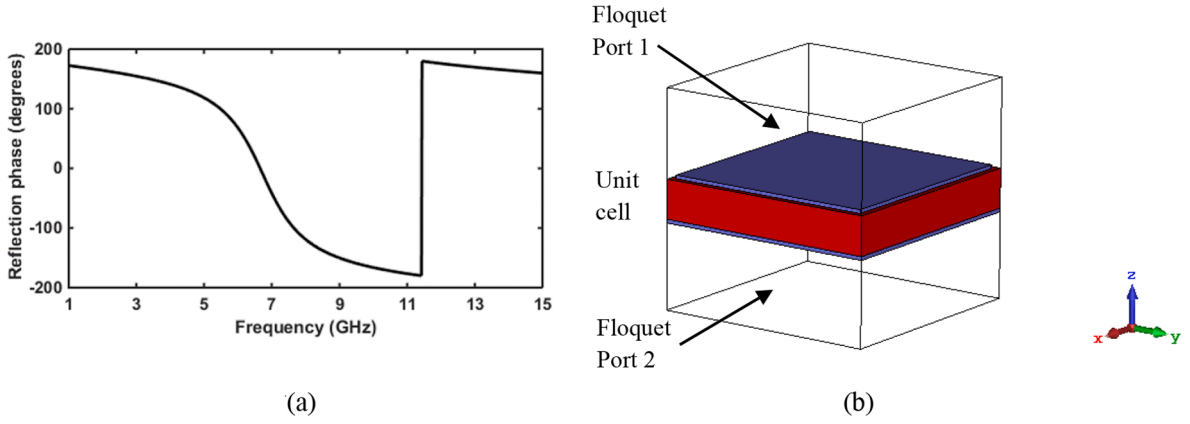

Fig. 3. (a) The reflection phase angle variation versus frequency, (b) The simulation model expressing the boundary conditions of the unit cell.

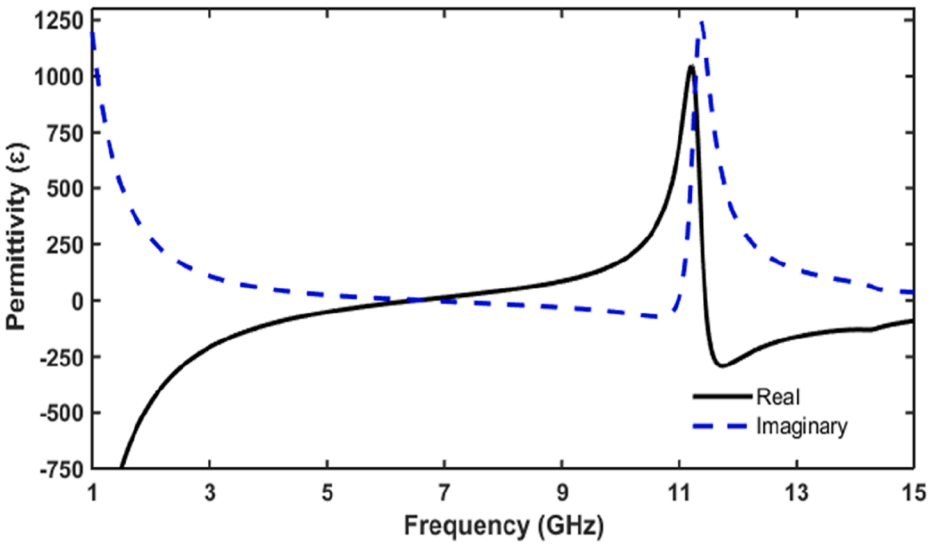

Fig. 4. Change of imaginary and real parts of effective permittivity of the designed MM structure with frequency calculated by using S-parameters found in simulations.

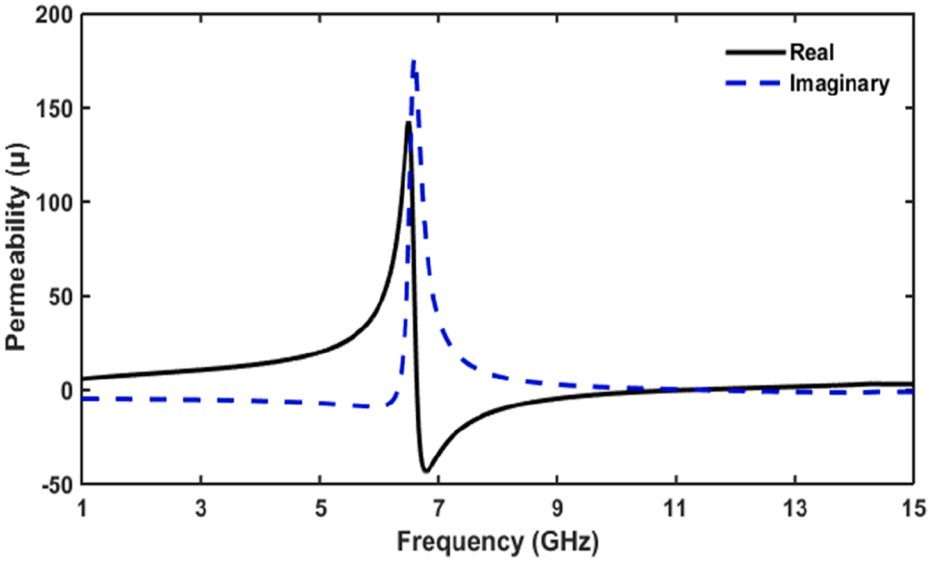

Fig. 5. Change of imaginary and real parts of permeability of the designed MM structure with frequency calculated by using S-parameters found in simulations.

frequencies below 6.8 GHz and above 11.5 GHz. Similarly, in Fig. 5, the imaginary part of the permeability is 0 in the whole frequency band except the very narrow frequency band around 6.8 GHz. At this frequency, permeability has resonance behavior. On the other hand, the real part of the permeability is positive at frequencies lower than 6.8 GHz and it is negative at frequencies above 6.8 GHz up to 11.5 GHz. If Figs. 4 and 5 are compared it is seen that at frequencies lower than 6.8 GHz and bigger than 11.5 GHz real part of the designed MM permittivity is negative and at frequencies between 6.8 GHz and 11.5 GHz real part of the designed MM permeability is negative. In other words, either real part of the designed MM permittivity or real part of the designed MM permeability is negative in the whole frequency regime spanning from 1 GHz till 15 GHz. This is an expected result and justifies the structure used as a metamaterial.

3. Simulation and measurement results

3.1. Reflection coefficient results

The analyses were started with simulations of the designed antenna without the MM structure behind it. Reflection coefficient (S_{11}) of the antenna was calculated by means of a 3D EM simulation software. After the simulations, measurements were obtained with the prototype antenna by using vector network analyzer (Rohde Schwartz ZNB). Variation of the S_{11} values with frequency calculated and measured in the UWB frequency region is shown in Fig. 7. Despite the slight changes in the reflection coefficient at some frequencies and the shifts in resonance frequencies, still there is a good match between the calculated and the measured coefficient values. In addition, more importantly, impedance bandwidth ($S_{11} \leq -10$ dB) covering the UWB frequency region is maintained in both the simulation and measurement. In Fig. 7, from the measurement results it is seen that the antenna has a wide frequency band spanning from 1.9 GHz to 13.4 GHz.

After that, the simulations and measurements of the antenna were

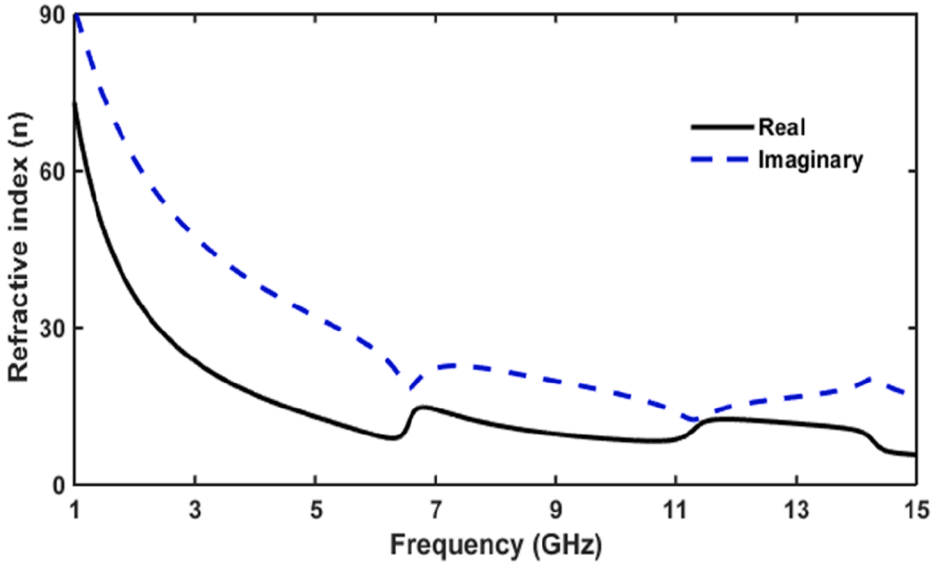

Fig. 6. Change of imaginary and real parts of refractive index of the designed MM structure with frequency calculated by using S-parameters found in simulations.

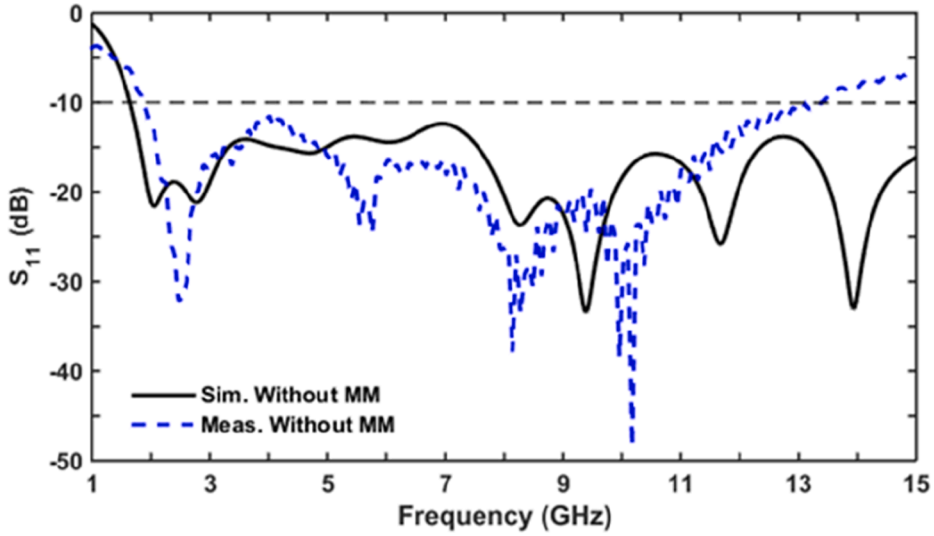

Fig. 7. Change of S_{11} parameter calculated in simulations and measured in experiments with frequency for the designed antenna without the MM structure behind it in free space.

then repeated with the MM structure placed behind the antenna as shown in Fig. 2(a). Fig. 8 shows the measured and simulated S_{11} reflection coefficient parameter of the proposed antenna with the MM. It is clear from the S_{11} curves that the antenna with the MM structure has a wide operating bandwidth in the UWB frequency region. While the simulated impedance bandwidth in which S_{11} is lower than or equal to −10 dB extends from 3.55 GHz to 13 GHz, in measurements the impedance bandwidth starts approximately from 3.7 GHz and ends at 13 GHz. The measured S_{11} parameter has partial overruns above −10 dB in the frequency range from 3.95 to 4.55 GHz, but the maximum S_{11} value is below −6.8 dB. Fig. 8 shows that although the bandwidth of the designed antenna integrated with the MM at its back is slightly narrowed, it still has a wide bandwidth, i.e., 8.45 GHz frequency bandwidth spanning from 4.55 GHz till 13 GHz, in the UWB frequency regime.

In addition, reflection coefficient calculations were repeated by removing circular parasitic patch from the antenna ground at its back. However, other parts of the design including the MM structure still exist without any change. By this way, it is aimed to observe parasitic patch effect on antenna performance. For easy comparison, in Fig. 9 variation of S_{11} parameter for the designed antenna without the circular parasitic patch on the antenna's ground is shown together with the variation of S_{11} parameter for the designed antenna with the circular parasitic patch on its ground. In the figure, it is seen that while the S_{11} value is above −10 dB in the frequency range of 3.87 GHz and 4.12 GHz for the antenna without a circular parasitic patch on the MM structure, this value has fallen below −10 dB with the integration of the parasitic patch. Therefore, the use of the parasitic patch increased the designed antenna bandwidth.

3.2. *Realized gain, FBR and radiation pattern results*

After obtaining reflection coefficient simulations and measurements, similar analyses were done for the maximum realized gain, FBR, and radiation pattern of the designed antenna with and without the MM structure placed behind the antenna. Maximum realized gain of the proposed antenna with and without the MM structure at the back of the antenna calculated in the simulations over the operating frequency band are shown in Fig. 10. In the figure it is seen that except at some

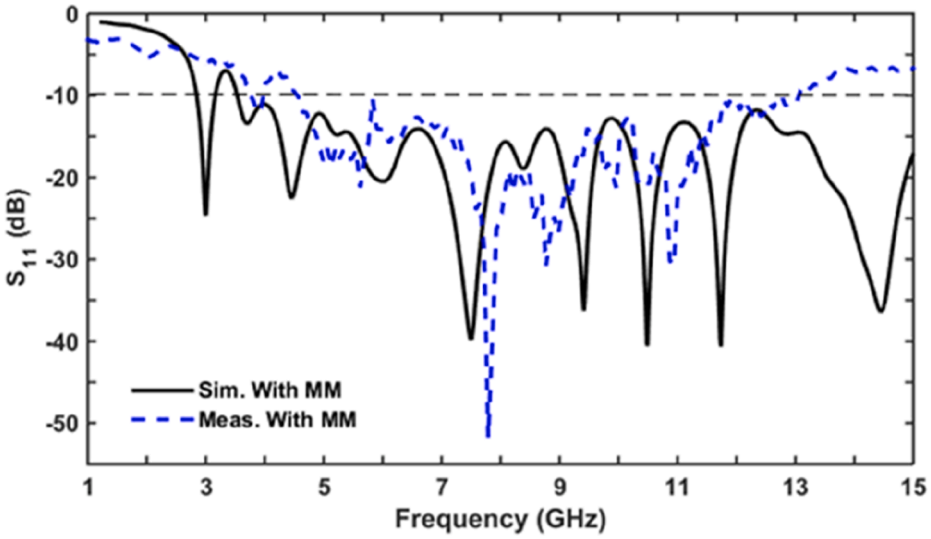

Fig. 8. Change of S_{11} parameter calculated in simulations and measured in experiments with frequency for the designed antenna with the MM structure behind it in free space.

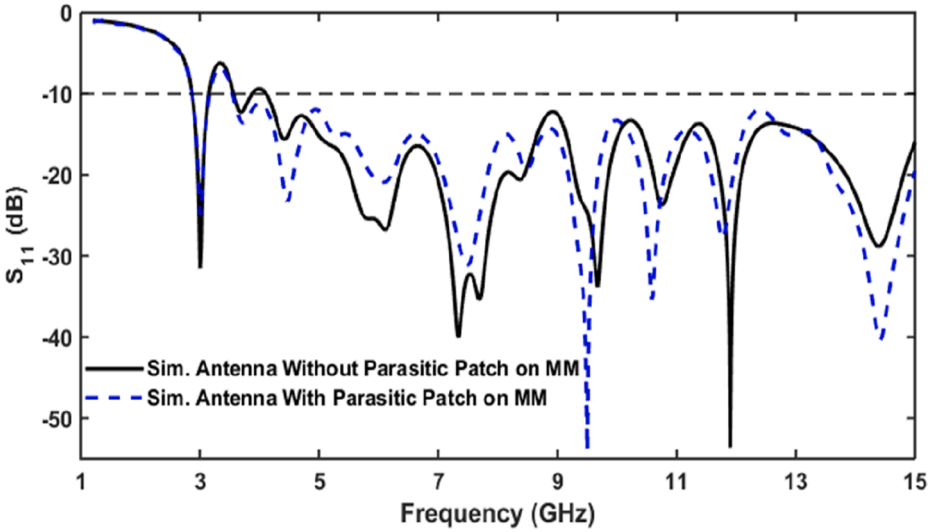

Fig. 9. Change of S_{11} parameter calculated in simulations with frequency for the designed antenna with and without the circular parasitic patch on the antenna's ground but with the MM structure at the back.

frequencies in the operating frequency band the maximum realized gain of the antenna increases with placement of the designed MM structure to its back. However, at frequencies in the range of 8.9 GHz and 10.4 GHz gain of the antenna with the designed MM structure at its back falls below the gain of the antenna without the MM structure at its back. The decrease in the maximum realized gain of the antenna in the frequency range of 8.9 GHz and 10.4 GHz is because of the specified frequency range being outside the effective frequency range of the designed MM and the existence of the felt spacer between the antenna and the MM structure. Effective frequency range of the MM is the frequency range at which reflection phase is between -90° and $+90^{\circ}$ (see Fig. 3(a)). Nevertheless, realized gain of the designed antenna with the MM structure at its back is calculated to be minimum 1.4 dBi at 10.1 GHz frequency.

In Fig. 11, on the other hand, variations of the FBR value over the ultra-wide operating frequency band calculated in the simulations for the proposed antenna with and without the MM structure in free space are presented. From the curves it is observed that as the designed MM structure is integrated to the back of the antenna, the FBR value significantly increases over the entire operating frequency band, which is due to increased antenna directivity and reduced back radiation. As seen in the figure, the FBR value of the proposed antenna without the MM structure in the operating frequency band varies between −1.85 dB and 7 dB, whereas the FBR value of the proposed antenna with the MM structure at its back ranges between 16 dB and 23.5 dB.

Furthermore, far-field radiation patterns of the proposed antenna with and without the MM structure in free space calculated in simulations at 4, 7.5 and 10.5 GHz frequencies are presented in polar coordinate system in Fig. 12. If the radiation patterns in each subfigure are compared, it is seen that the directivity increases, and the back radiation decreases with placement of the designed MM structure to the back of the antenna. As a result, less EM waves impinge on and absorbed by the body.

3.3. On body performance of the antenna with and without the MM structure

When a wearable antenna is used on a human body, part of

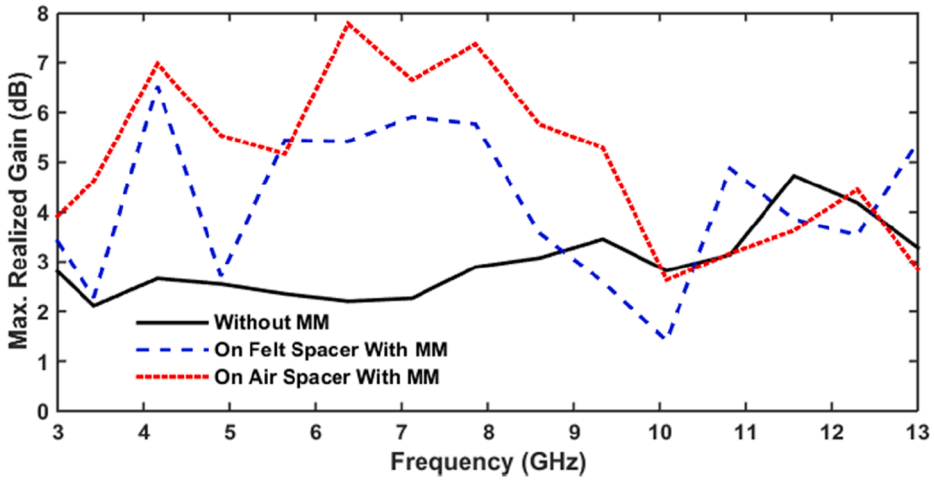

Fig. 10. Change of the maximum realized gain with frequency calculated in simulations for the designed antenna without the MM structure and with the MM structure on air and felt spacers.

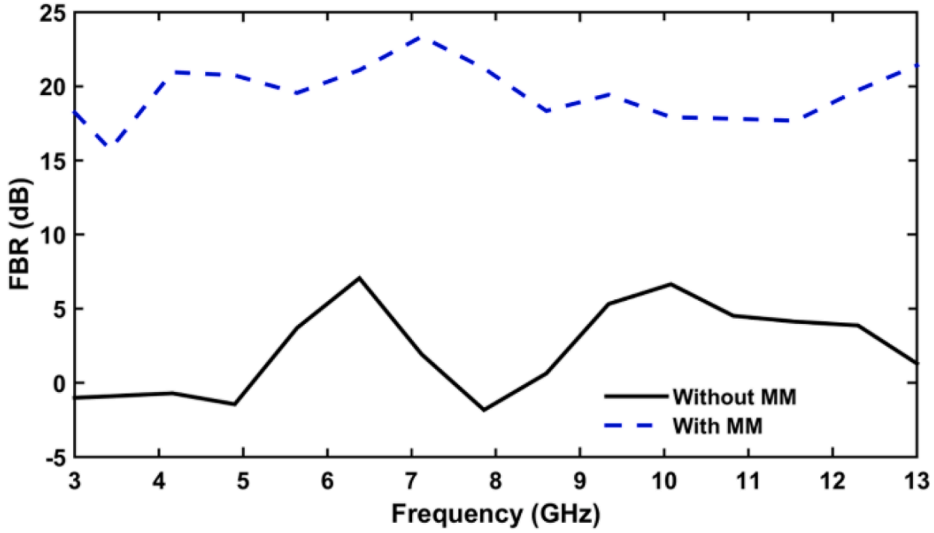

Fig. 11. Change of the FBR value with frequency calculated in simulations for the designed antenna with and without the MM structure behind it in free space.

electromagnetic energy radiated from the antenna is absorbed and part of it is reflected by the body. Therefore, it is necessary to figure out performance change of the designed antenna and its effects to the human body in the case of on body usage. Human body is modelled as cubic body model in the simulation software, and we used this model in our simulations. The body model is shown in Fig. 13. As seen in the figure, the body model consists of 4 layers of human body tissues that are skin, fat, muscle, and bone from outer side to inner. The skin, fat, muscle, and bone layers are 1.7 mm, 8 mm, 10 mm, and 3.3 mm thick, respectively, and the modeled geometry has sizes of 120 mm, 130 mm, and 23 mm in total. The layer thicknesses in the modeled body are the same with those reported in literature [23]. In addition, in simulations, the material density and dielectric constant values of body tissues are taken from the values defined in the material library of the CST (2014) software. Material density and dielectric constant values used in the simulations at various frequencies are given in Table 2. As seen, both real and imaginary parts of dielectric constant values of the body tissues change with frequency.

We placed the designed antenna and the MM on the human body model and obtained simulations. To investigate effect of the proposed MM structure simulations were repeated without the MM structure between the designed antenna and the body model. For fair comparison, in both cases, i.e., with and without the MM structure, the distance between the antenna and the body model was kept being constant at 3.34 mm. In addition, we obtained measurements with the manufactured antenna prototype and the prototype of the MM structure. In our experiments, we placed the designed antenna and the MM on our body. The distance between the antenna and our body in the experiments is 3.34 mm (see Fig. 2(a), where total thickness of the spacer felt, metasurfaces, MM felt, and MM ground equals to 3.34 mm), which is the same with the distance between the antenna and the body model in the simulations. As in the simulations, we also repeated the measurements with and without the prototype MM structure. Again for fair comparisons, in the experiments without the MM structure distance between the antenna and our body is set to be equal to 3.34 mm. Change of S_{11} parameters with frequency calculated in the simulations and measured in the experiments for the designed antenna in free space and on body model with and without the MM structure are shown in Figs. 14 and 15, respectively. In Fig. 10 it is observed that, despite shifts in resonance frequencies and changes in S_{11} values, the ultra-wide operating frequency band of the designed antenna without the MM structure maintains in the case of on body usage. In Fig. 15, on the other hand, changes between the graphs of free space and on body cases are lower than those exist in Fig. 14. This is because of the fact that when the designed

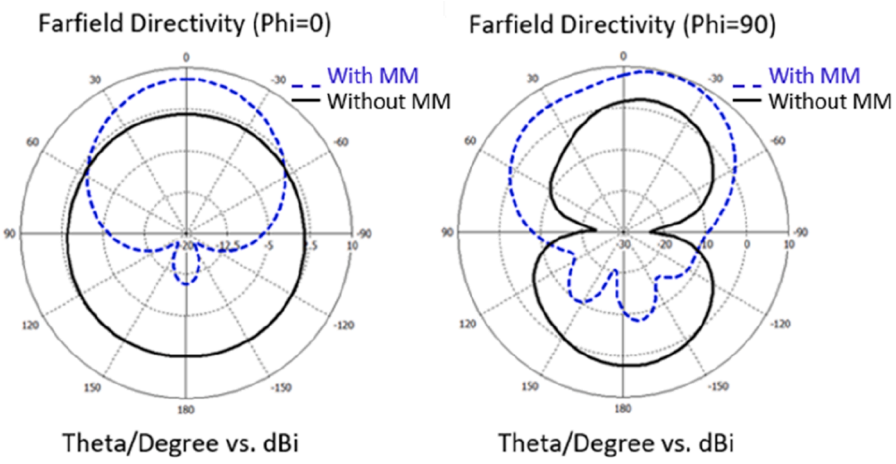

(a) 4 GHz

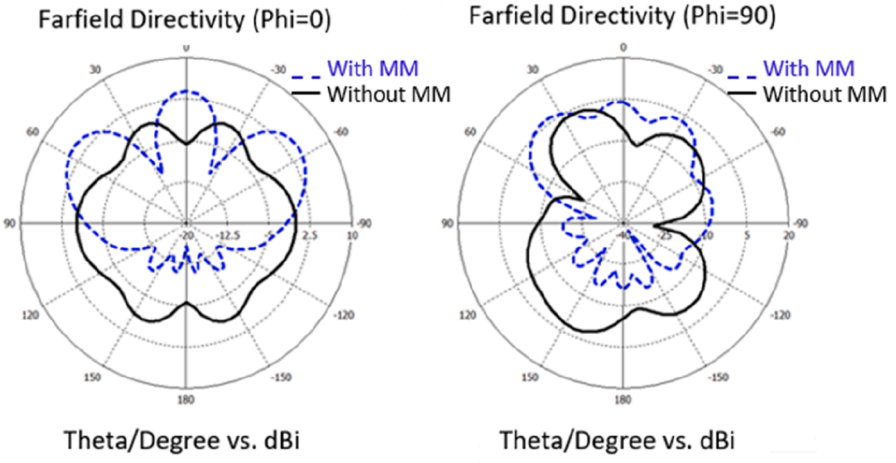

(b) 7.5 GHz

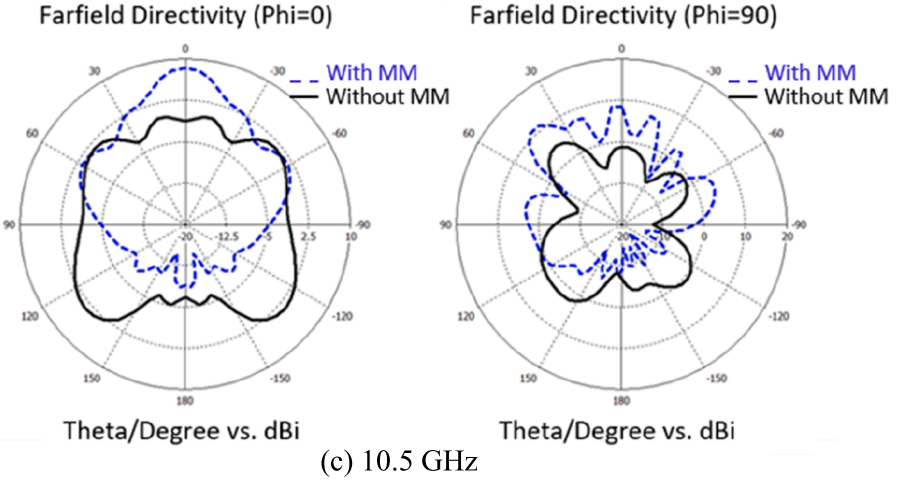

(c) 10.5 GHz

Fig. 12. Far-field radiation patterns of the designed antenna with and without the MM structure at its back in polar coordinate system at different angels (Phi:0 and Phi:90) calculated in simulations at a frequency of (a) 4 GHz, (b) 7.5 GHz, and (c) 10.5 GHz.

antenna is used with the MM structure behind it, the antenna is isolated from the body by the designed MM structure.

Finally, to investigate the effect of antenna radiation on a human body SAR values of the designed antenna with and without the MM structure were calculated at frequencies of 4, 7.5, and 10.5 GHz. SAR is a measurement that determines the rate of energy absorbed by the human body due to exposure to the radio frequency (RF) electromagnetic field. SAR is expressed as the absorbed power per unit tissue mass and its unit is W/kg [24]. In general, it is averaged over a small sample volume or over the entire body. However, in wearable antenna applications the whole-body average is not taken into account in the SAR value calculations. SAR is used to measure the level of exposure to body areas in the RF frequency ranges between 100 kHz and 10 GHz [25]. In the calculations antenna input power is set to be 0.5 W in accordance with the IEEE C95.3 standards. Also, in the simulations cubic human tissue model (see Fig. 12) with 10 g mass, which is a standard value, is used. The

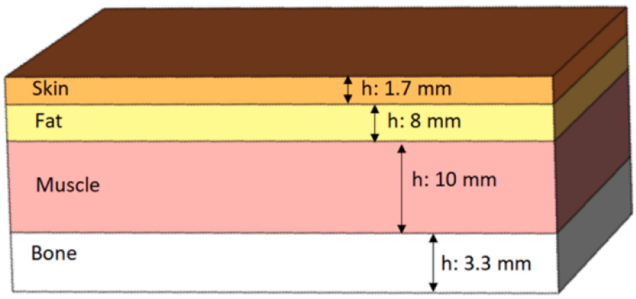

Fig. 13. Perspective view of cubic body tissue model used in the simulations. Here, 4 layers of the body tissues are represented with different colors and they are labeled. Also, thickness of each layer is indicated by an arrow and the thickness values are written on the arrows.

safety limit is 2 W/kg for a 10 g tissue. SAR values of the proposed antenna calculated in simulations for 10 g human body tissue at different frequencies with and without the designed MM structure at the back of the antenna are illustrated in Figs. 16 and 17, respectively. In Fig. 16 it is seen that the maximum SAR value of the antenna without the MM structure is found to be 6.27, 2.23 and 1.94 W/kg at frequencies of 4 GHz, 7.5 GHz, and 10.5 GHz, respectively. These SAR values exceed the 2 W/kg limit set for a 10 g tissue in European standards. In Fig. 17 on the other hand, the maximum SAR value of the antenna with the designed MM structure is calculated to be 0.067, 0.107 and 0.070 W/kg at frequencies of 4 GHz, 7.5 GHz, and 10.5 GHz, respectively. These SAR values are very low compared to the values found for the antenna without the MM structure, and they are in compliance with the European standards.

The proposed antenna design with the MM structure is compared with the antennas reported in literature in Table 3 in terms of operating frequency bandwidth, flexibility, dimensions, and gain characteristics. In a wearable antenna, all of these parameters and characteristics are very important. As seen in the table, our designed antenna has the lowest thickness. Although footprint of a wearable antenna is important, its thickness is one of the main concerns in design and usage. Among the antennas that are compared with our design in the table, the antennas reported in [20,26,27] have thickness closest to the thickness of our designed antenna. However, operating frequency bands of these antennas are much narrower than the frequency band of our designed antenna. The antennas mentioned in [28] and [29] have operating frequency bands that are comparable with or wider than the frequency band of our designed antenna. However, these antennas have high profile structures, i.e., with thickness of 14.8 mm and 20 mm, and they are not suitable to be used as wearable antennas. As far as we know, 4.68 mm thickness of the designed antenna with MM structure at its back is the lowest thickness reported in literature for UWB full-textile wearable antennas with MM structure. As can be seen from the reference studies, it is not easy to design a low profile UWB antenna with an integrated MM structure. Therefore, because of its low profile, being manufactured by fully textile materials that enables complete flexibility, and UWB operating frequency regime, the designed antenna with MM structure provides a significant advantage for wearable antenna applications. In addition, as seen in the table, 6 dBi peak gain of the antenna is high enough for wearable antenna applications compared to the studies exist in literature.

4. Conclusion

In this study, an UWB low-profile wearable antenna with MM structure at its back is proposed for WBAN applications. The designed

Table 2
Material density and dielectric constant values of the human body tissues used in the simulations.

Tissue	Density (kg/m^3)	Dielectric Constant					
		4 GHz		7.5 GHz		10.5 GHz	
		Real Part	Imaginary Part	Real Part	Imaginary Part	Real Part	Imaginary Part
Skin	1100	35.3	10.5	30.6	9.4	28.4	8
Fat	910	5.1	0.83	4.6	0.8	4.4	0.8
Muscle	1041	50	13.07	43.3	15.2	38.8	14.6
Bone	1850	10.3	3.3	8.5	3.2	7.4	2.6

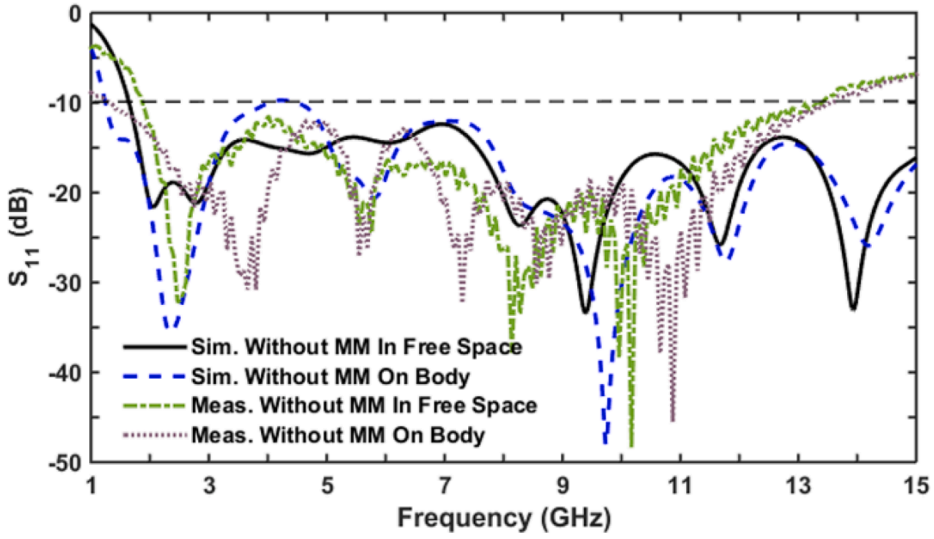

Fig. 14. Change of S_{11} parameter calculated in simulations and measured in experiments with frequency for the designed antenna without the MM structure behind it in free space and on body.

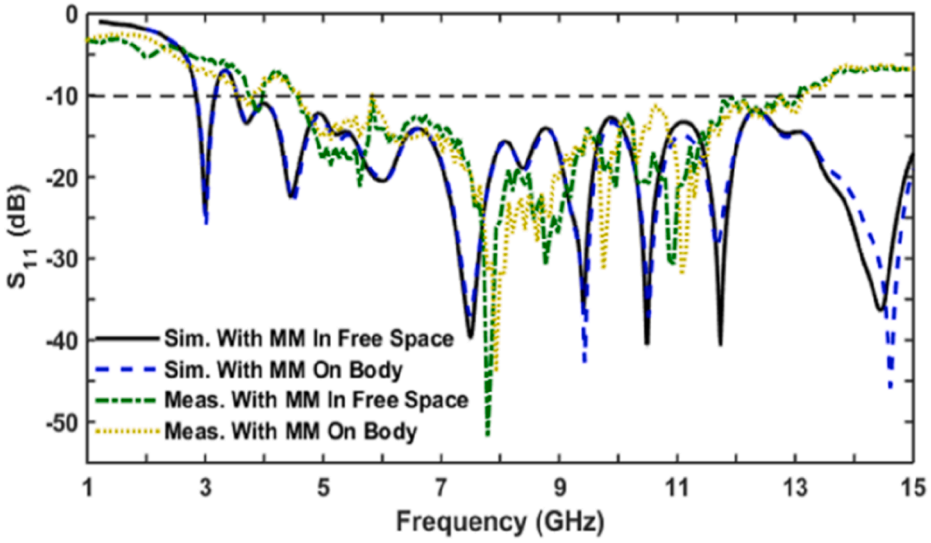

Fig. 15. Change of S_{11} parameter calculated in simulations and measured in experiments with frequency for the designed antenna with the MM structure behind it in free space and on body.

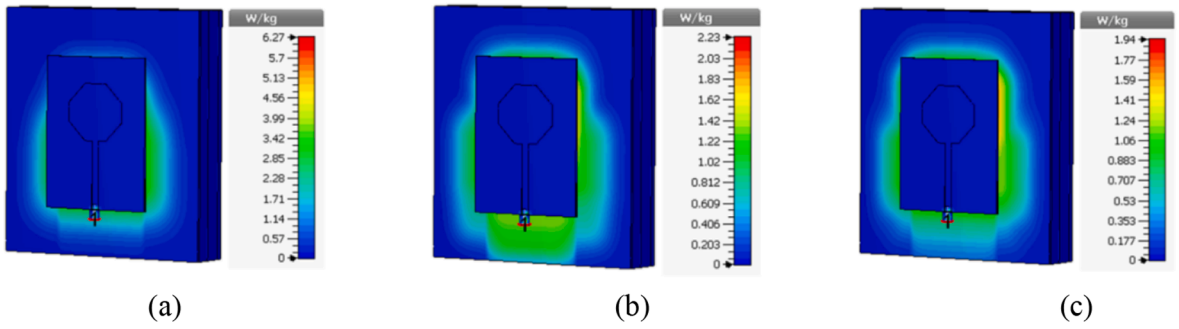

Fig. 16. SAR values of the designed antenna without the MM structure at its back calculated in simulations for 10 g human body tissue at a frequency of (a) 4 GHz, (b) 7.5 GHz, and (c) 10.5 GHz.

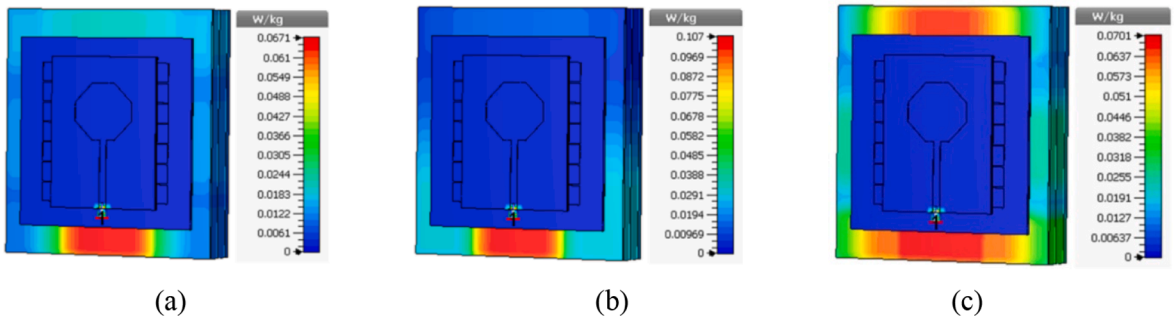

Fig. 17. SAR values of the designed antenna with the MM structure at its back calculated in simulations for 10 g human body tissue at a frequency of (a) 4 GHz, (b) 7.5 GHz, and (c) 10.5 GHz.

antenna has hexagonal geometry at its top side responsible from radiation. On the other hand, at the back side of the antenna there are rectangular shape ground plane and circular parasitic patch, which decrease back radiation and increase FBR value of the antenna while allowing large bandwidth. In addition, to further decrease back radiation of the antenna and increase its directivity MM structure consisting of metasurface cells aligned in a square lattice is proposed and implemented to the back of the antenna. The designed antenna and the MM structure are both made of full-textile materials. Performance of the designed antenna was investigated with the simulations and measurements both with and without the MM structure. Results show that the designed antenna with the MM structure at its back has an ultra-wide impedance bandwidth of 8.45 GHz extending from 4.55 GHz to 13 GHz in the UWB frequency regime. Also, from the results it is observed that the gain, directivity, and FBR of the antenna increase by implementing the designed MM structure to the back of the antenna. In the simulations far-field radiation patterns of the antenna at different frequencies with and without the MM structure at its back were calculated, too. From the pattern graphs, it is deduced that the directivity increases and the back radiation decreases with placement of the designed MM

Table 3
Operating frequency band, substrate type, dimensions, and peak gain of our proposed antenna design with the MM structure at its back and the wearable antennas reported in literature.

Ref. No	Operating frequency band (GHz)	Substrate type (flexible/ rigid)	Size of Antenna with MM (mm^2)	Thickness of Antenna with MM (mm)	Peak Gain (dB/ dBi)
[30]	2.4 ISM	Flexible	50 × 50	9.5	4.12 dBi
[31]	2.3–3/4–5.3	Flexible	77 × 87	8	7.3 dB
[26]	2.4–2.5	Flexible	100 × 100	6.5	2.42 dB
[32]	2.45/5.5	Flexible	102 × 102	7	5.2 dB
[20]	1.85–3.15	Flexible	84 × 162.25	6.5	3.38 dB
[27]	5.7–11	Flexible	46 × 46	5.8	8 dBi
[28]	2.6–12	rigid	72 × 72	14.8	9.9 dBi
[12]	2.45 /5.8	Flexible	42 × 63	8	7.8 dB
[29]	2.5–13.8	Flexible	52.5 × 52.5	20	9 dB
Proposed	4.55–13	Flexible	100 × 100	4.68	6 dBi

structure to the back of the antenna which results in less EM waves impinging on and absorbed by the body during on body usages of the antenna.

Furthermore, to investigate radiation effect of the designed antenna on a human body SAR values of the antenna with and without the designed MM structure at its back in free space and on the body model were calculated at different frequencies. It is seen that the peak SAR values decrease substantially with placement of the MM structure behind the antenna such that the decrease was calculated to reach 98.3%. The peak SAR value of the designed antenna with the MM structure on the body model was calculated to be. 0.067, 0.107, and 0.070 W/kg at frequencies of 4 GHz, 7.5 GHz, and 10.5 GHz, respectively. These SAR values are very low compared to the maximum SAR limit of 2 W/kg identified in the European standards for 10 g tissue. In addition, on body simulations and experiments demonstrate that the designed antenna with the MM structure at its back maintains ultra-wide operating impedance bandwidth in UWB frequency region.

The proposed system structure that consists of the designed antenna and the MM structure have very low profile. As far as we know, 4.68 mm thickness of the designed system is the lowest thickness reported in literature for UWB full-textile wearable antennas with MM structure. We believe that with all these advantages including having very low profile and low SAR, manufactured by fully textile materials that provides complete flexibility, and operating on ultra-wide frequency band, the designed antenna with the MM structure at its back is promising to be used for WBAN applications.

Declaration of Competing Interest

The authors declare that they have no known competing financial interests or personal relationships that could have appeared to influence the work reported in this paper.

References

[1] Shakhirul MS, Jusoh M, Sahadah A, Nor CM, Rahim HA. Embroidered wearable textile antenna on bending and wet performances for UWB reception. Microw Opt Technol Lett 2014;56:2158–63.
[2] Hassan S, Shehab SH. Evaluation of an ultra wideband (UWB) textile antenna in the vicinity of human body model for WBAN applications. In: 2015 IEEE int. WIE conf. electr. comput. eng. IEEE; 2015. p. 195–8.
[3] Yan S, Poffelie LAY, Soh PJ, Zheng X, Vandenbosch GAE. On-body performance of wearable UWB textile antenna with full ground plane. In: 2016 10th Eur. conf. antennas propag. IEEE; 2016. p. 1–4.
[4] Mohandoss S, Palaniswamy SK, Thipparaju RR, Kanagasabai M, Naga BRB, Kumar S. On the bending and time domain analysis of compact wideband flexible monopole antennas. AEU-Int J Electron Commun 2019;101:168–81.
[5] Boyes SJ, Soh PJ, Huang Y, Vandenbosch GAE, Khiabani N. On-body performance of dual-band textile antennas. IET Microwaves, Antennas Propag 2012;6:1696–703.
[6] Gao G-P, Yang C, Hu B, Zhang R-F, Wang S-F. A wearable PIFA with an all-textile metasurface for 5 GHz WBAN applications. IEEE Antennas Wirel Propag Lett 2018;18:288–92.
[7] Bin Jalil ME, Abd Rahim MK, Samsuri NA, Murad NA, Majid HA, Kamardin K, et al. Fractal koch multiband textile antenna performance with bending, wet conditions and on the human body. Prog Electromagn Res 2013;140:633–52.
[8] Srivastava G, Mohan A, Chakrabarty A. Compact reconfigurable UWB slot antenna for cognitive radio applications. IEEE Antennas Wirel Propag Lett 2016;16:1139–42.
[9] Hong Y, Tak J, Choi J. An all-textile SIW cavity-backed circular ring-slot antenna for WBAN applications. IEEE Antennas Wirel Propag Lett 2016;15:1995–9.
[10] Fcc FCC. First report and order on ultra-wideband technology. Washington, DC, USA: FCC; 2002.
[11] Salvado R, Loss C, Gonçalves R, Pinho P. Textile materials for the design of wearable antennas: a survey. Sensors 2012;12:15841–57.
[12] Mersani A, Lotfi O, Ribero J. Design of a textile antenna with artificial magnetic conductor for wearable applications. Microw Opt Technol Lett 2018;60:1343–9.
[13] Yalduz H, Koç B, Kuzu L, Turkmen M. An ultra-wide band low-SAR flexible metasurface-enabled antenna for WBAN applications. Appl Phys A 2019;125:609.
[14] Ashyap AYI, Zainal Abidin Z, Dahlan SH, Majid HA, Saleh G. Metamaterial inspired fabric antenna for wearable applications. Int J RF Microw Comput Eng 2019;29:e21640.
[15] Abdu A, Zheng H, Jabire HA, Wang M. CPW-fed flexible monopole antenna with H and two concentric C slots on textile substrate, backed by EBG for WBAN. Int J RF Microw Comput Eng 2018;28:e21505.
[16] Alemaryeen A, Noghanian S. Crumpling effects and specific absorption rates of flexible AMC integrated antennas. IET Microwaves, Antennas Propag 2017;12:627–35.
[17] Varamini G, Keshtkar A, Daryasafar N, Naser-Moghadasi M. Microstrip Sierpinski fractal carpet for slot antenna with metamaterial loads for dual-band wireless application. AEU-Int J Electron Commun 2018;84:93–9.
[18] DicCbshfsE J, Abd Rahim MK, Samsuri NA, Salim HAM, Ali MF. Embroidered fully textile wearable antenna for medical monitoring applications. Prog Electromagn Res 2011;117:321–37.
[19] Malekpoor H, Jam S. Improved radiation performance of low profile printed slot antenna using wideband planar AMC surface. IEEE Trans Antennas Propag 2016;64:4626–38.
[20] Hussin EFNM, Soh PJ, Jamlos MF, Lago H, Al-Hadi AA, Rahiman MHF. A wideband textile antenna with a ring-slotted AMC plane. Appl Phys A 2017;123:46.
[21] Xu HX, Wang GM, Qi MQ. Hilbert-shaped magnetic waveguided metamaterials for electromagnetic coupling reduction of microstrip antenna array. IEEE Trans Magn 2012;49(4):1526–9.
[22] Xu HX, Wang GM, Liang JG, Qi MQ, Gao X. Compact circularly polarized antennas combining meta-surfaces and strong space-filling meta-resonators. IEEE Trans Antennas Propag 2013;61(7):3442–50.
[23] Tripathi S, Mohan A, Yadav S. A performance study of a fractal UWB antenna for on-body WBAN applications. Microw Opt Technol Lett 2017;59:2201–7.
[24] Jin J. Electromagnetic analysis and design in magnetic resonance imaging, Vol. 1. CRC Press; 1998.
[25] Wu Wei, Wu Zhaohui, Yu Taekyung, Jiang Changzhong, Kim Woo-Sik. Recent progress on magnetic iron oxide nanoparticles: synthesis, surface functional strategies and biomedical applications. Sci Technol Adv Mater 2015;16:2.
[26] Lago H, Soh PJ, Jamlos MF, Shohaimi N, Yan S, Vandenbosch GAE. Textile antenna integrated with compact AMC and parasitic elements for WLAN/WBAN applications. Appl Phys A 2016;122:1059.
[27] Liu X, Di Y, Liu H, Wu Z, Tentzeris MM. A planar windmill-like broadband antenna equipped with artificial magnetic conductor for off-body communications. IEEE Antennas Wirel Propag Lett 2015;15:64–7.
[28] Kumar Pandey G, Shankar Singh H, Kumar Meshram M. Investigations of triple band artificial magnetic conductor back plane with UWB antenna. Microw Opt Technol Lett 2016;58:1900–6.
[29] Wang F, Arslan T. A wearable ultra-wideband monopole antenna with flexible artificial magnetic conductor. In: 2016 Loughbrgh. antennas propag. conf., IEEE; 2016. p. 1–5.
[30] Agarwal K, Guo Y-X, Salam B. Wearable AMC backed near-endfire antenna for on-body communications on latex substrate. IEEE Trans Compon, Packag Manuf Technol 2016;6:346–58.
[31] Mantash M, Tarot A-C, Collardey S, Mahdjoubi K. Investigation of flexible textile antennas and AMC reflectors. Int J Antennas Propag 2012;2012.
[32] Chahat N, Zhadobov M, Sauleau R, Mahdjoubi K. Improvement of the on-body performance of a dual-band textile antenna using an EBG structure. In: 2010 Loughbrgh. antennas propag. conf. IEEE; 2010. p. 465–8.

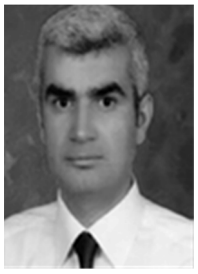

Husnu Yalduz received his B.S. degree and M.S. degree in electrical and electronics engineering from the Nigde University (Nigde) and Yüzüncüyıl University (Van) in Turkey, respectively. Currently, He is working as a lecturer in Department of Vocational School, Hitit University, Corum, Turkey. He is doing his Ph.D in electrical and electronics engineering, Erciyes University, Kayseri, Turkey. His research interests are the antennas and propagations; ultra-wideband (UWB), RFID, body area network (BAN).

Timucin Emre Tabaru received the M.S. and Ph.D. degrees in the Department of Electrical-Electronics Engineering from Erciyes University, Kayseri, Turkey, in 2014 and 2018, respectively. He is working as a lecturer at The Clinical Engineering Research and Application Center, Erciyes University. His current research interests are fiber optic sensors, optical signal processing, photoacoustic detection, photonic sensors, biomedical optics and electro-optical instruments, antennas and propagations.

Veli Tayfun Kilic received the B.S., M.S., and Ph.D. degrees from Bilkent University, Ankara, Turkey, in 2009, 2011, and 2017, respectively, all in electrical and electronics engineering. In February 2018, he joined Abdullah Gul University, Kayseri, Turkey, where he is currently an Assistant Professor at the Department of Electrical and Electronics Engineering. His research interests include radio frequency systems, near-field and far-field electromagnetic coupling, radio frequency antennas, plasmonic antennas, and radio frequency circuits.

Mustafa Turkmen received his M.S. and Ph.D. degrees from the Erciyes University, both in electrical and electronics engineering, in 2003 and 2009, respectively. He worked for Boston University as a visiting research assistant professor between 2009 and 2012. He is working as an associate professor in the electrical and computer engineering Department at Erciyes University (Turkey). His current research interests include microwave printed circuits, and patch antennas for wireless communication applications, metamaterials, nanoplasmonics, and their applications in chemical and biological sensing, and optical communication. Dr. Turkmen is a recipient of the Graduate and Postdoctoral Research Fellowships from the scientific and technological research council of Turkey (TUBITAK).